



INSTITUT NATIONAL DE RECHERCHE EN INFORMATIQUE ET EN AUTOMATIQUE

## *Accurate Model Reduction of Transient Flows*

Bernardo Galletti — Alessandro Bottaro — Charles-Henri Bruneau — Angelo Iollo

**N° 5676**

Septembre 2005

\_\_\_\_\_ Thème NUM \_\_\_\_\_

A large blue rectangle occupies the lower half of the page. Overlaid on it is a large, light gray stylized letter 'R'. To the right of the 'R', the words 'Rapport de recherche' are written in a white serif font. A horizontal gray brushstroke is positioned below the text.

*Rapport  
de recherche*





## Accurate Model Reduction of Transient Flows

Bernardo Galletti <sup>\*</sup>, Alessandro Bottaro <sup>†</sup>, Charles-Henri Bruneau <sup>‡</sup>,  
Angelo Iollo <sup>‡</sup>

Thème NUM — Systèmes numériques  
Projet MC2

Rapport de recherche n° 5676 — Septembre 2005 — 18 pages

**Abstract:** Some applications of a precise method to model the transient dynamics of large scale structures in the laminar flow past a bluff body are presented. The flow is described using empirical eigenfunctions obtained by “proper orthogonal decomposition” and the models are constructed projecting the Navier-Stokes equations onto such eigenfunctions. The linear terms in the expansion coefficients as well as in the control inputs are adjusted to exactly mimic some reference solutions. Applications shown concern the development of flow instabilities leading to vortex shedding and the dynamics of the vortex wake under external actuation.

**Key-words:** model reduction, proper orthogonal decomposition, Navier-Stokes equations

<sup>\*</sup> DIASP, Politecnico di Torino, 10129 Torino, Italy

<sup>†</sup> DIAM, Università di Genova, 16145 Genova, Italy

<sup>‡</sup> MAB -Université Bordeaux 1 et MC2 - INRIA Futurs, 33405 Talence, France

## Réduction précise de modèles d'écoulements instationnaires

**Résumé :** On présente quelques applications d'une méthode précise pour modéliser la dynamique instationnaire de structures à grande échelle, relative à un écoulement laminaire décollé. L'écoulement est décrit en utilisant des fonctions propres empiriques obtenues par la "décomposition orthogonale aux valeurs propres (POD)". Les modèles sont construits à partir de la projection des équations de Navier-Stokes sur ces fonctions propres. Des termes linéaires mettant en jeu les coefficients du développement et les termes de contrôle sont ajustés pour reproduire exactement quelques solutions de référence. Les applications concernent le développement des instabilités dans un écoulement avec un sillage tourbillonnaire, et la dynamique du sillage soumis à des actionneurs.

**Mots-clés :** modèles réduits, décomposition orthogonale aux valeurs propres, équations de Navier-Stokes

## 1 Introduction

Finite dimensional models involving a limited number of degrees of freedom can greatly simplify the analysis of fluid flows. The dynamics can be interpreted in terms of a small number of coherent structures that evolve and interact with one another. Low order models are also of practical interest since they can be used as “plant models” for control purposes.

Using the proper orthogonal decomposition technique (POD) [13] one can extract from an existing database of flow field snapshots, a set of orthogonal eigenfunctions. For a given number of these eigenfunctions, the average  $l^2$  projection error of a flow snapshot is minimized by construction. As a consequence, when the flow energy is concentrated in large scale vortical structures, a small number of POD eigenfunctions captures a large fraction of the total kinetic energy of the flow. This may not always be the case since there exist applications where, even though there are large structures present in the flow, the energy spreads over so many scales that there is little hope to obtain a practical low dimensional representation [23]. In contrast, flows past bluff bodies seem to be well represented by  $O(10)$  empirical eigenfunctions [8, 14, 15] and hence are good candidates for investigations of low dimensional models.

Even when the flow is amenable to a low dimensional description, it is not obvious that a reliable dynamical model can be obtained. In principle it suffices to project the Navier-Stokes equations onto the POD eigenfunctions by a classical Galerkin approach. This way, however, one is faced with some typical problems of Galerkin approximations:

- i)* how to account for boundary conditions (and eventually boundary controls);
- ii)* how to device a closure term that accounts for the unresolved modes;
- iii)* how to provide adequate numerical stabilization.

The last two issues are closely related because usually dissipation of energy occurs mainly on the level of scales which are poorly resolved. However, in the literature they are often considered separately.

In the Cornell low order dynamical system [1] of the turbulent boundary layer, an Heisenberg model accounted for the unresolved scales and a dissipation coefficient was tuned in order to obtain qualitatively correct results. However, to be able to use the model results for a case not previously investigated by direct numerical simulation (DNS), the amount of dissipation to be added should be known *a priori*. Along these lines it was proposed [5] to adjust the dissipation parameter so that the energy budget for each POD mode is balanced. This way it was possible to diminish the error between the dynamical system predictions and the DNS projection over the POD modes. Nevertheless, an exponential divergence in time between the DNS and the model results persists.

In parallel studies, it was recognized that a straightforward POD-Galerkin approximation of a model problem - a scalar linear advection equation - was numerically unstable [11, 12]. In that case there was no question of lack of dissipation because of missing scales; it was a pure numerical effect. Moreover, it was shown that the POD-Galerkin projection for such a simple case is equivalent to a finite difference centered spatial discretization, and that the effect of truncating the Galerkin expansion was at most that of enlarging the stability bounds of the POD-Galerkin scheme. In addition, it was proved that selecting an appropriate Sobolev

norm in the definition of the empirical eigenfunctions as well as in the Galerkin projection, the low order models obtained displayed better stability properties, as recently confirmed in [19].

Clearly, low Reynolds number simulations suffer much less from numerical instabilities because of physical viscosity, and hence the corresponding POD models are not affected by instabilities if a sufficient number of POD modes are taken into account [8, 14]. Even for such cases, though, the long term dynamics predicted by the low order model may deviate significantly from reference DNS results as shown in [20]. As a remedy a dissipative model based on spectral viscosity was proposed therein. The cut-off parameters were selected based on bifurcation analysis, *i.e.*, by matching the attractor of the low order model to that predicted by DNS.

The idea of fitting the POD model results to those of DNS is attractive since it may solve some of the physical modeling issues as well as the problem of numerical drifts. The main property that such an approach should retain to be of practical interest is that of being predictive, *i.e.*, it should be applicable to cases other than those used to build the model itself. In this sense in [9] it was proposed to calibrate the linear term in the Galerkin model resulting from projecting the Navier-Stokes equations over the POD modes, in order to achieve a best fit for a number of reference time-dependent flow solutions. In particular, it was shown that such calibration leads to a model that correctly reproduced the main flow features for Reynolds numbers other than those from which the model was derived. Similar approaches have been recently investigated for moderately to complex flows [2, 6, 16].

The purpose of this paper is to improve the calibration procedure presented in [9] and extend it in order to model the transient dynamics of coherent structures. Two test cases are considered: the development of a flow instability leading to vortex shedding and the dynamics of a vortex wake under the effect of transverse flow due to wall-mounted actuators.

## 2 Model reduction

We consider the flow around a square cylinder symmetrically placed between semi-infinite parallel walls (Fig. 1). The inlet velocity profile is parabolic. For a blockage ratio  $L/H$  of 0.125, this flow is believed to be two-dimensional and laminar as long as the Reynolds number based on the square side  $L$  is below 255 [3, 7, 17, 22]. The flow field data are obtained by numerical integration of the incompressible Navier-Stokes equations. The integration scheme as well as the computational parameters, like channel length and cylinder position, are the same as used in [9]. We refer the reader to that study for the computational details and for the validation of the numerical results. Unless otherwise stated, all the quantities considered are non dimensional: the reference values for the normalization are the length  $L$  of the side of the square cylinder, the center-line velocity at the inlet section  $U$ , the dynamic pressure  $\rho U^2$  and the time scale  $T_{ref} = L/U$ .

The velocity field database is arranged as a set of  $N$  vectors  $\{\mathbf{U}^{(1)}, \mathbf{U}^{(2)}, \dots, \mathbf{U}^{(N)}\}$ , where each vector represents a snapshot of the velocity field at a given time. Let us subtract

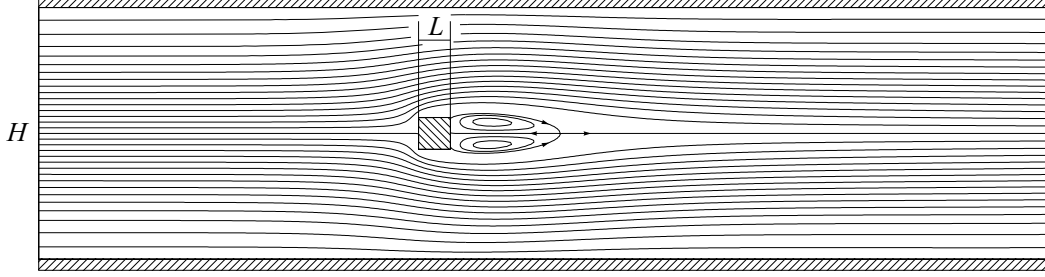


Figure 1: Definition of the geometry and streamlines of the unstable, steady solution  $\bar{\mathbf{u}}(\mathbf{x})$  at  $Re = 66$ .

the steady, unstable solution<sup>1</sup>  $\bar{\mathbf{U}}$  from each snapshot and consider the new set of filtered snapshots  $\mathbf{W}^{(n)} = \mathbf{U}^{(n)} - \bar{\mathbf{U}}, n = 1, \dots, N$ . The aim is to find a low dimensional subspace of  $\mathcal{L} = \text{span}\{\mathbf{W}^{(1)}, \mathbf{W}^{(2)}, \dots, \mathbf{W}^{(N)}\}$  that gives the best approximation of  $\mathcal{L}$ . To this end we define a unit norm vector  $\phi$  that has the same structure of the snapshots and the largest mean square projection on the elements of  $\mathcal{L}$ . Following Sirovich's ideas [21] we express  $\phi$  as a linear combination of the snapshots,  $\phi = \sum_{n=1}^N b_n \mathbf{W}^{(n)}$ , which leads to the eigenproblem  $\mathbf{R} \mathbf{b} = \lambda \mathbf{b}$ , where  $R_{ks} = \mathbf{W}^{(k)T} \mathbf{W}^{(s)}$  and  $\mathbf{b} = [b_1, b_2, \dots, b_N]^T$ . The solution of the eigenproblem yields  $N$  eigenvectors  $\phi_n$  (the discrete POD modes) that form a complete orthonormal set for  $\mathcal{L}$ . The discrete instantaneous velocity can be expanded in terms of the discrete POD eigenmodes:  $\mathbf{u}(\mathbf{x}, t) = \bar{\mathbf{u}}(\mathbf{x}) + \sum_{n=1}^{N_r} a_n(t) \phi_n(\mathbf{x})$ . The main property of this basis is that most of the flow energy is captured using a number  $N_r \ll N$  of functions  $\phi_n$ .

## 2.1 POD-Galerkin Model

An accurate model of the developing instability is obtained by a Galerkin projection of the incompressible Navier-Stokes equations over the POD modes. The resulting low order model is

$$\begin{aligned} \dot{a}_r(t) &= (A'_r + A''_r) + (C'_{kr} + C''_{kr}) a_k(t) - B_{ksr} a_k(t) a_s(t) \\ a_r(0) &= (\mathbf{u}(\mathbf{x}, 0), \phi_r) \end{aligned} \quad (1)$$

where the Einstein summation convention is used and all the subscripts run from 1 to  $N_r$ . The coefficients  $A'_r$ ,  $B_{ksr}$  and  $C''_{kr}$  derive directly from the Galerkin projection of the Navier-Stokes equations onto the POD modes and are defined by

$$\begin{aligned} B_{ksr} &= (\phi_k \cdot \nabla \phi_s, \phi_r) \\ C''_{kr} &= -(\bar{\mathbf{u}} \cdot \nabla \phi_k, \phi_r) - (\phi_k \cdot \nabla \bar{\mathbf{u}}, \phi_r) + (\Delta \phi_k, \phi_r) / Re \\ A''_r &= -(\bar{\mathbf{u}} \cdot \nabla \bar{\mathbf{u}}, \phi_r) + (\Delta \bar{\mathbf{u}}, \phi_r) / Re \end{aligned}$$

<sup>1</sup>A description of how this base flow is obtained is given in Section 3.

where  $(\cdot, \cdot)$  is the canonical  $l^2$  inner product; the terms  $A'_r$  and  $C'_{kr} a_k(t)$  are added in order to model the interaction of the unresolved modes with the resolved ones. They also take into account the effect of the pressure drop along the channel. By setting  $A'_r = A_r - A''_r$  and  $C'_{kr} = C_{kr} - C''_{kr}$  system (1) reads

$$\begin{aligned} \dot{a}_r(t) &= f_r(a_1, \dots, a_{N_r}, A_r, C_{kr}) = A_r + C_{kr} a_k(t) - B_{ksr} a_k(t) a_s(t) \\ a_r(0) &= (\mathbf{u}(\mathbf{x}, 0), \phi_r) \end{aligned} \quad (2)$$

In view of the orthogonality of the POD modes, the inner product of the  $i$ -th snapshot and the  $r$ -th mode represents the reference value of coefficient  $a_r(t)$  computed at the time  $t_i$ , that is  $\hat{a}_r(t_i) = (\mathbf{W}^{(i)}, \phi_r)$ . Since the snapshots of the flow are  $N$ , there will be a discrete set of  $N$  reference values for each amplitude  $a_r(t)$ . We can pass from the discrete to the continuous setting in the time variable by defining  $\hat{a}_r(t)$  as the spline interpolating the set of points  $\{[t_1, \hat{a}_r(t_1)], \dots, [t_N, \hat{a}_r(t_N)]\}$ .

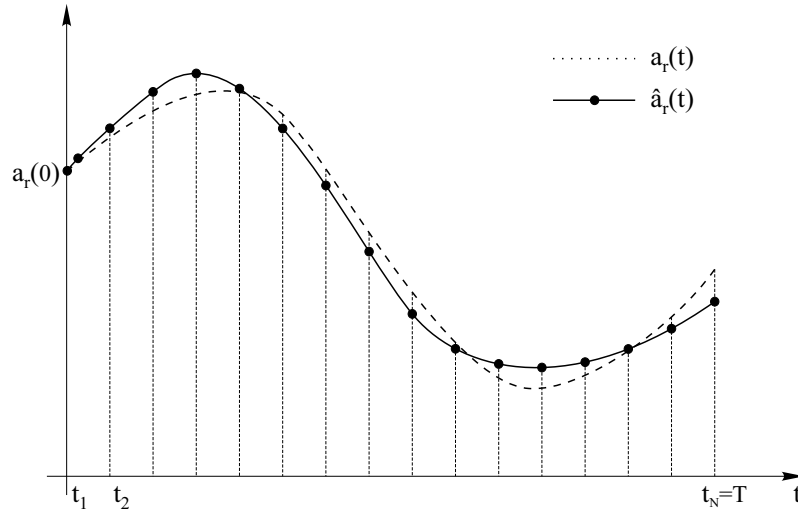


Figure 2: Projection vs. prediction

At this point the coefficients  $A_r, C_{kr}$  can be found so that the amplitude coefficients  $a_r(t)$ , computed by solving (2) (dashed line in the sketch of figure 2), are as close as possible to the corresponding reference amplitudes  $\hat{a}_r(t)$  (solid line in the sketch of figure 2). Recalling that  $T = t_N$ , this objective is reached by minimizing the functional

$$\int_0^T \sum_{r=1}^{N_r} (a_r(t) - \hat{a}_r(t))^2 dt$$



under the constraints (2). The previous problem is equivalent to finding the unconstrained extremum of the functional:

$$\mathcal{J} = \int_0^T \sum_{r=1}^{N_r} (a_r(t) - \hat{a}_r(t))^2 dt + \int_0^T b_k [\dot{a}_k(t) - A_k - C_{lk} a_l(t) + B_{lsk} a_l(t) a_s(t)] dt.$$

where  $b_k$  is the appropriate Lagrange multiplier. To this end the vanishing of the Fréchet derivatives of  $\mathcal{J}(a_r(t), b_r(t), A_r, C_{kr})$  with respect to all of its arguments must be imposed. This leads to the following optimality problem

$$\begin{cases} \dot{a}_r(t) = A_r + C_{kr} a_k(t) - B_{ksr} a_k(t) a_s(t) \\ a_r(0) = (\mathbf{u}(\mathbf{x}, 0), \phi_r) \end{cases} \quad \text{direct problem} \quad (3)$$

$$\begin{cases} -\dot{b}_r(t) = [C_{rk} - (B_{lrk} + B_{rlk}) a_l(t)] b_k(t) - 2[a_r(t) - \hat{a}_r(t)] \\ b_r(T) = 0 \end{cases} \quad \text{adjoint problem} \quad (4)$$

$$\begin{cases} \int_0^T b_r(t) dt = 0 \\ \int_0^T a_k(t) b_r(t) dt = 0 \end{cases} \quad \text{optimality conditions} \quad (5)$$

where all of the subscripts go from 1 to  $N_r$ . These equations are discretized with a pseudo-spectral collocation method along the  $t$  axis. The functions  $a_r(t)$ ,  $b_r(t)$  and  $\hat{a}_r(t)$  are sampled at the  $N_t$  Gauss-Lobatto points  $t_i = T/2(1 - \xi_i)$  with  $\xi_i = \cos \pi(i - 1)/(N_t - 1)$  and  $i = 1, \dots, N_t$ , that is  $a_{ir} = a_r(t_i)$ ,  $b_{ir} = b_r(t_i)$  and  $\hat{a}_{ir} = \hat{a}_r(t_i)$ . An interpolation is performed to retrieve the values of the functions away from the nodal points  $t_i$ , more precisely

$$\begin{aligned} a_r(t) &\approx \sum_{j=1}^{N_t} \psi_j \left(1 - \frac{2}{T}t\right) a_{jr} \\ b_r(t) &\approx \sum_{j=1}^{N_t} \psi_j \left(1 - \frac{2}{T}t\right) b_{jr} \\ \hat{a}_r(t) &\approx \sum_{j=1}^{N_t} \psi_j \left(1 - \frac{2}{T}t\right) \hat{a}_{jr} \end{aligned}$$

where  $\xi = 1 - 2t/T$  and  $\psi_j(\xi)$  are the Lagrangian interpolating polynomials based on the nodes  $\xi_i$ . The time derivatives of the first two interpolated functions at the nodal values are then

$$\begin{aligned} \dot{a}_r(t_i) &\approx -\frac{2}{T} \sum_{j=1}^{N_t} \frac{d\psi_j}{d\xi} \Big|_{\xi_i} a_{jr} = \sum_{j=1}^{N_t} D_{ij} a_{jr}, \\ \dot{b}_r(t_i) &\approx -\frac{2}{T} \sum_{j=1}^{N_t} \frac{d\psi_j}{d\xi} \Big|_{\xi_i} b_{jr} = \sum_{j=1}^{N_t} D_{ij} b_{jr}. \end{aligned} \quad (6)$$

The differentiation matrix can be found in [4] and is equal to

$$D_{ij} = -\frac{2}{T} \left. \frac{d\psi_j}{d\xi} \right|_{\xi_i} = -\frac{2}{T} \begin{cases} \frac{c_i}{c_j} \frac{(-1)^{j+i}}{\xi_i - \xi_j} & j \neq i \\ -\frac{1}{2} \frac{\xi_i}{1 - \xi_i^2} & j = i \neq 1, N_t \\ \frac{2(N_t - 1)^2 + 1}{6} & j = i = 1 \\ -\frac{2(N_t - 1)^2 + 1}{6} & j = i = N_t \end{cases}$$

with  $c_1 = c_{N_t} = 2$  and  $c_2 = \dots = c_{N_t-1} = 1$ .

The optimality condition can be rewritten in terms of the interpolated functions as follows

$$\int_0^T a_k(t) b_r(t) dt \approx \sum_{i=1}^{N_t} \sum_{j=1}^{N_t} a_{ik} I_{ij} b_{jr} \quad (7)$$

where the integrals

$$I_{ij} = \int_0^T \psi_i(\xi) \psi_j(\xi) d\xi \quad \text{with } i, j = 1, \dots, N_t$$

are calculated by means of Legendre quadrature. Finally, by virtue of (6) and (7), equations (3-5) are discretized as follows

$$\begin{aligned} a_{1r} &= a_r(0) & r &= 1, \dots, N_r \\ D_{ij} a_{jr} - A_r - C_{lr} a_{il} + B_{lsr} a_{il} a_{is} &= 0 & i &= 2, \dots, N_t, \quad r = 1, \dots, N_r \\ D_{ij} b_{jr} + C_{rs} b_{is} - (B_{lrs} + B_{rls}) a_{il} b_{is} - 2[a_{ir} - \hat{a}_{ir}] &= 0 & i &= 1, \dots, N_t - 1, \quad r = 1, \dots, N_r \\ b_{N_t r} &= 0 & r &= 1, \dots, N_r \\ \mathbf{1}_i I_{ij} b_{jr} &= 0 & r &= 1, \dots, N_r \\ a_{ik} I_{ij} b_{jr} &= 0 & k &= 1, \dots, N_r \quad r = 1, \dots, N_r \end{aligned}$$

where  $\mathbf{1}$  is a  $N_t$ -dimensional array of ones. These are  $2N_t N_r + N_r + N_r^2$  algebraic equations in the  $2N_t N_r + N_r + N_r^2$  unknowns and are solved with a Newton method which converges rapidly. The number  $N_t$  must be large enough to produce a good description of the high frequency behavior of the amplitude coefficients, consequently it should be increased with the increase of  $N_r$ .

The former procedures can be interpreted as a calibration of the model on the given database.

### 3 Low dimensional modeling of the developing instability

The frequency and amplitude of the oscillations of the flow in the wake are computed at several values of the Reynolds number between 60 and 70. Extrapolating to 0 the wake oscillation amplitude as a function of the Reynolds number, it was found that - in the present configuration - the critical value for the onset of periodic flow is approximately  $Re = 57$ .

We consider a numerical database of the flow developing out of the unstable, steady solution at  $Re = 66$ . After initialization from rest, we identify the symmetric field having minimal time residual, as the steady unstable solution, see figure 1. From there on, the DNS indicates that the transient lasts about 95 units of time, until the limit cycle solution is attained.

Our intent is to simulate the initial part of the transient originating from the steady, unstable solution at  $Re = 66$ . Beginning from such a solution a simulation lasting 40 units of time was performed. A model like the one of equation (2) can be deduced from such a database, with the unknowns  $A_r, C_{kr}$  calculated according to the procedure described above.

The number of POD modes used for the model is  $N_r = 4$ , which yields the following error in terms of reconstructed flow energy:

$$\frac{1}{N} \sum_{i=1}^N \frac{\|\mathbf{w}^{(i)} - \sum_{n=1}^{N_r} (\mathbf{w}^{(i)}, \phi_n) \phi_n\|}{\|\mathbf{u}^{(i)}\|} = 0.005. \%$$

In Fig. 3(a) the solution of the model in terms of the time evolution of the coefficients  $a_i(t)$

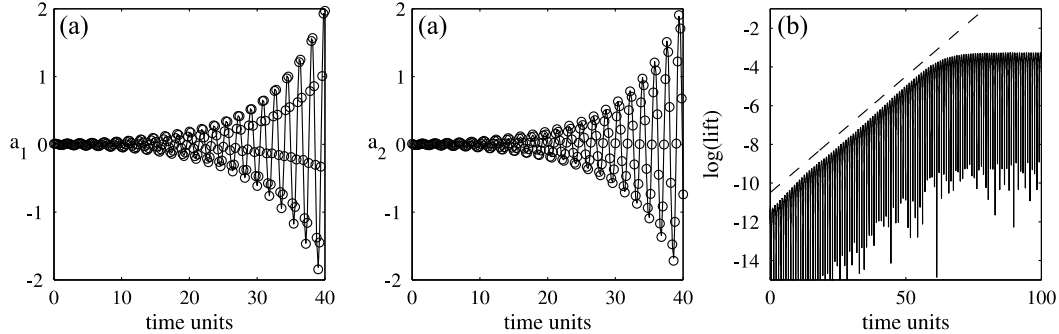


Figure 3: (a) Prediction of the model calibrated between 0 and 40 time units of the transient: comparison between the mode amplitudes of model integration (solid lines) and the projection of the numerical simulation over the corresponding modes (circles). (b) Logarithm of the absolute value of the lift in the transient regime (solid line) and a line (dashed) of slope  $\text{Re}(\lambda_1)/T_{ref}$ .

is compared to the reference Navier-Stokes solution projected over the POD modes. The model is able to exactly reproduce the dynamics of the considered part of the transient.

In perfect analogy with what one would do in a stability study using a full order model, we compute the growth rate of the absolute instability using equation (2). The equation is linearized about the equilibrium state  $a_r(0) = 0$  with  $r = 1, \dots, N_r$  which corresponds to the unstable solution of the steady Navier-Stokes equations for  $Re = 66$ . Expanding  $f_r$  as a power series about this equilibrium point and neglecting the second order terms one obtains:  $\dot{a}_r(t) = f_r(0, A_r, C_{kr}) + J_{rj} a_j(t)$  where  $J_{rj} = (\partial f_r / \partial a_j)_0 = C_{jr}$ . From  $\dot{a}_r(0) \simeq 0$  it follows that  $A_r \simeq 0$ ; this fact is confirmed numerically since the coefficient  $A_r$  found is of order  $10^{-4}$ . As a result  $f_r(0, A_r, C_{kr}) \simeq 0$ , so that the linearized state equation reads

$$\mathbf{a}_t(t) = \mathbf{J} \mathbf{a}(t). \quad (8)$$

The solution is

$$\mathbf{a}(t) = \mathbf{Q} \exp(\mathbf{\Lambda} t) \mathbf{Q}^{-1} \mathbf{a}(0) \quad (9)$$

with  $\mathbf{a}(t) = [a_1(t), \dots, a_{N_r}(t)]^T$ ,  $\mathbf{\Lambda}$  the  $N_r \times N_r$  diagonal matrix corresponding to the eigenvalues of  $\mathbf{J} = \{J_{rj}\}_{1 \leq r, j \leq N_r}$  and  $\mathbf{Q}$  the  $N_r \times N_r$  matrix whose columns are the corresponding right eigenvectors. The numerical values are  $\lambda_1 = 0.03 + 0.74i$ ,  $\lambda_2 = 0.03 - 0.74i$ ,  $\lambda_3 = -0.16$ ,  $\lambda_4 = -0.09$  and

$$\mathbf{Q} = \begin{bmatrix} 0.71 & 0.71 & -0.10 & -0.02 \\ -0.00 + 0.70i & -0.00 - 0.70i & -0.03 & -0.10 \\ -0.00 - 0.00i & -0.00 + 0.00i & -0.32 & -0.92 \\ -0.00 - 0.00i & -0.00 + 0.00i & -0.94 & -0.37 \end{bmatrix}$$

with  $i = \sqrt{-1}$ . There are two complex conjugate eigenvalues with positive real part,  $\lambda_1$  and  $\lambda_2$ . The eigenvectors pertinent to  $\lambda_1$  and  $\lambda_2$  are just the first two POD modes (with a phase shift of  $\pi/4$ ). We conclude that the only unstable modes relative to this flow are represented by the first and second POD modes. It is interesting to remark that the imaginary parts of  $\lambda_1$  and  $\lambda_2$  correspond to a non-dimensional frequency of  $\text{Im}(\lambda_1)/(2\pi) = 0.119$  whereas the non-dimensional vortex shedding frequency of the fully developed flow is 0.124. Unsurprisingly, the growth rate of the instability is very close to that predicted by the real part of  $\lambda_1$ , as illustrated in Fig. 3(b). We conclude that the most energetic unsteady POD modes, extracted from a DNS of the transient state, give a reliable representation of the absolute instability of this flow.

In order to assess the capability of the POD-Galerkin model to give good predictions even for times longer than those upon which the model was built, a time integration of the model itself has been performed beyond  $t = 40$  and up to a time of 100, corresponding to the fully developed flow. The amplitudes so-computed have been compared to the projections of the flow snapshots taken from the integration range onto the given POD modes. The snapshots between the time units 40 and 100 are reconstructed by the POD modes relevant to the interval 0-40 with an average error of about 5%. In Fig. 4(a) a comparison

is shown between the first amplitude coefficient resulting from model integration and the corresponding reference amplitude obtained by projection. A perfect agreement between prediction and projection inside the POD extraction interval (denoted with  $T_{POD}$  in the figure) is observed. Outside of this range, the solution is accurately extrapolated for several shedding cycles, but for larger times a slight phase drift as well as an error in the oscillation amplitude prediction is remarked. One can notice, however, that the model is able to predict the length of the transient, as both the computed and the projected amplitudes saturate in approximately the same time. The above procedure has been repeated by extracting a POD base from a database of 145 snapshots between the time instants 28.4 and 35.6, and by calibrating a four dimensional POD-Galerkin model over the same time interval. The results depicted in Fig. 4(b) are quite similar to the previous ones, showing that the same amount of information can be captured by taking snapshots from a narrow time interval in the first part of the transient.

### 3.1 Absolute unstable mode estimation

Let us now compare the most unstable mode obtained by the above reduced model to the one obtained by the method proposed in [10], where the full order problem, *i.e.* the incompressible Navier-Stokes equations, linearized about the steady unstable solution  $\bar{\mathbf{U}}$ , is used. To this end let  $\mathbf{L}$  denote the linearization of the Navier-Stokes discretization operator in space, once the incompressibility constraint is satisfied. The resulting semidiscretization valid in the vicinity of  $\bar{\mathbf{U}}$  can be written as

$$\psi_t = \mathbf{L} \psi \quad (10)$$

where  $\psi(t) = \mathbf{U}(t) - \bar{\mathbf{U}}$  is a column vector which contains the grid values of the velocity components arranged with the same rules as they are organized in the snapshots vectors. The dimensions of  $\psi$  and  $\mathbf{L}$  are  $2M \times 1$  and  $2M \times 2M$  respectively, with  $M$  the number of grid points. The solution of equation (10) can be written

$$\psi(t) = \mathbf{P} \exp(\mathbf{\Sigma} t) \mathbf{P}^{-1} \psi_0 \quad (11)$$

where  $\psi_0$  is the initial condition corresponding to the steady unstable solution,  $\mathbf{\Sigma}$  is the diagonal matrix containing the eigenvalues of  $\mathbf{L}$  and  $\mathbf{P}$  is the matrix whose columns are the corresponding eigenvectors such that  $\mathbf{L}\mathbf{P} = \mathbf{P}\mathbf{\Sigma}$ .

Denote by  $\Phi$  the matrix whose columns are the POD modes retained in the model, arranged in vectors with the same rules as those by which the Navier-Stokes solution is arranged in  $\psi$ . We have  $\Phi^T \Phi = \mathbf{I}$  for the orthonormality of the POD modes. Let  $\mathbf{a}(t) = [a_1(t), \dots, a_{N_r}(t)]^T$  and  $\tilde{\psi}(t) = \Phi \mathbf{a}(t)$ , then equation (8) premultiplied by  $\Phi$  reads  $\tilde{\psi}_t \simeq \Phi \mathbf{J} \Phi^T \tilde{\psi}$ ; by comparing this equation with (10) the estimate  $\tilde{\mathbf{L}} = \Phi \mathbf{J} \Phi^T$  for the linearized Navier-Stokes operator  $\mathbf{L}$  is found. On the other hand, by construction, we have that  $\mathbf{J} = \Phi^T \mathbf{L} \Phi$ .

The solution of the linearized low-order model equation (9) matches exactly the projection of the Navier-Stokes data over the POD modes (Fig. 3). Hence, it can be used to

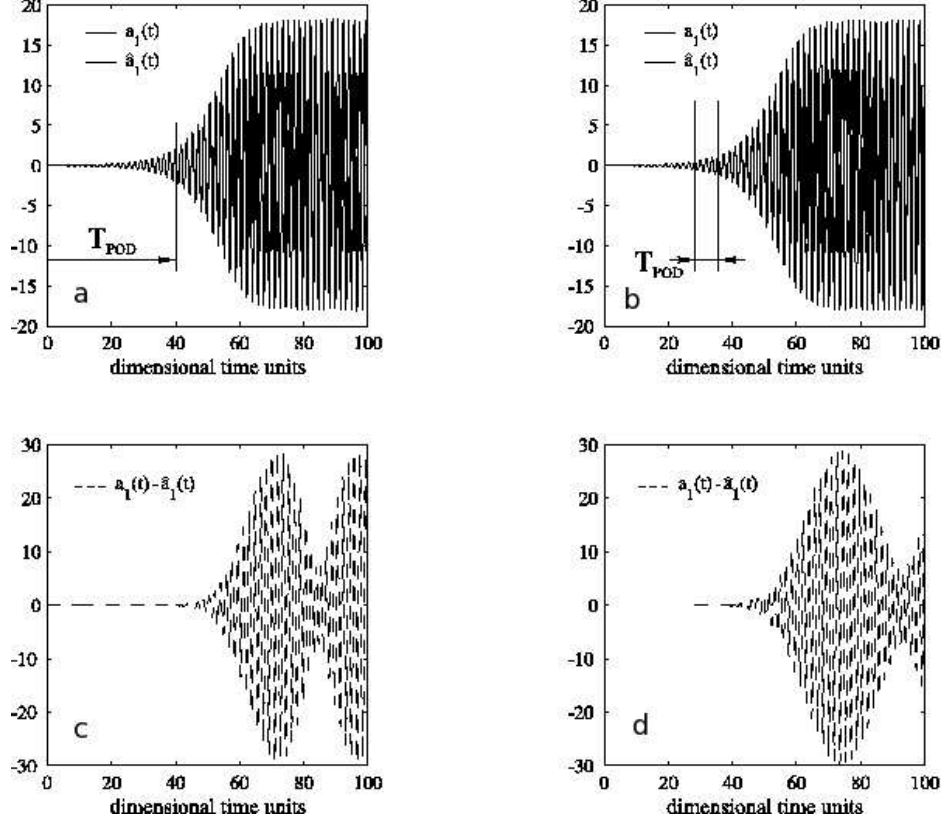


Figure 4: Prediction over the whole transient of the model calibrated on the time range 0-40: (a) comparison between the first mode amplitude from model integration  $a_1(t)$  (thick line) and numerical simulation  $\hat{a}_1(t)$  (thin line) and (c) their difference (dashed line). Prediction over the whole transient of the model calibrated on the time range 28.4–35.6: (b) comparison between the first mode amplitude from model integration  $a_1(t)$  (thick line) and numerical simulation  $\hat{a}_1(t)$  (thin line) and (d) their difference (dashed line).  $T_{POD}$  is the time interval where the POD are extracted

estimate the solution in the physical space by writing

$$\tilde{\psi}(t) = \Phi \mathbf{a} = \Phi \mathbf{Q} \exp(\mathbf{\Lambda} t) \mathbf{Q}^{-1} \Phi^T \psi_0 \quad (12)$$

We recall that  $\lambda_1$  and  $\lambda_2$  have positive real part and the corresponding unstable eigenvectors occupy the first two columns of  $\mathbf{Q}$ . Accordingly, we assume that the eigenvalues which correspond to the physical absolutely unstable mode are  $\sigma_1$  and  $\sigma_2$  ( $Re(\sigma_{1,2}) > 0$ ) with the physical unstable eigenvectors arranged in the first two columns of  $\mathbf{P}$ .

Let us denote with  $\mathcal{P}$  and  $\mathcal{P}^*$  the submatrices formed by the first two columns of  $\mathbf{P}$  and by the first two rows of  $\mathbf{P}^{-1}$  respectively. Similarly, let us denote with  $\mathcal{Q}$  and  $\mathcal{Q}^*$  the submatrices formed by the first two columns of  $\mathbf{Q}$  and by the first two rows of  $\mathbf{Q}^{-1}$ , respectively.

Then, by equalling the physical solution (11) to its reconstruction (12), after having neglected the decreasing exponentials, it follows that

$$\mathcal{P} \begin{bmatrix} e^{\sigma_1 t} & 0 \\ 0 & e^{\sigma_2 t} \end{bmatrix} \mathcal{P}^* \psi_0 = \Phi \mathcal{Q} \begin{bmatrix} e^{\lambda_1 t} & 0 \\ 0 & e^{\lambda_2 t} \end{bmatrix} \mathcal{Q}^* \Phi^T \psi_0.$$

Since  $\sigma_{1,2} = \lambda_{1,2}$ , we obtain  $\mathcal{P} = \Phi \mathcal{Q}$  and  $\mathcal{P}^* = \mathcal{Q}^* \Phi^T$ . In order to give a graphical representation of the reconstructed physical unstable eigenvector we have drawn in figure 5(b) the modulus of the first column of  $\mathcal{P}$ . It is interesting to make a comparison with the real unstable eigenvector obtained by solving the eigenproblem associated to the full linearized Navier-Stokes operator  $\mathbf{L}$ . The numerical value for the latter depicted in figure 5(a), have been kindly provided by Flavio Giannetti who has repeated for the current geometry the same kind of calculation performed in his work with Paolo Luchini for the case of the circular cylinder [10]. The agreement is satisfactory, confirming the validity of the POD-Galerkin approach in the study of the stability.

## 4 Low dimensional modeling of transversely forced flow

In this section we focus on the changes to be made in the POD-Galerkin model in order to obtain a proper simulation of the flow around the square cylinder when blowing/suction is performed along the channel walls. The velocity along the walls is everywhere zero except for two opposite segments next to the square where its transverse component varies in time, while remaining constant along the streamwise direction, that is  $\mathbf{u}(\mathbf{x}, t) = c(t)\mathbf{j}$  with  $\mathbf{x} \in \Gamma_c$  (see Fig. 6). The actuators are driven in opposite phases, i.e. at any time the velocity vector of the top actuator is equal in amplitude to that of the bottom actuator, so that the flow rate through the channel does not change.

Let us define with  $\bar{\mathbf{u}}'(\mathbf{x})$  our base state when  $c(t) = c^* = 0.1$ , obtained just like in the unforced case when the numerical simulation reaches a minimum value in the time residual. It can be observed that the filtered solution  $\mathbf{u}_c(\mathbf{x}) = \bar{\mathbf{u}}'(\mathbf{x}) - \bar{\mathbf{u}}(\mathbf{x})$  is such that  $\mathbf{u} = 0$  on  $\Gamma_{in}, \Gamma_w - \Gamma_c$  and  $\mathbf{u} = c^*\mathbf{j}$  on  $\Gamma_c$ . The velocity field of the system which has been forced with a generic control law  $c(t)$ , is expressed as in [18] according to the following expansion

$$\mathbf{u}(\mathbf{x}, t) = \bar{\mathbf{u}}(\mathbf{x}) + \frac{c(t)}{c^*} \mathbf{u}_c(\mathbf{x}) + \sum_{n=1}^{N_r} a_n(t) \phi_n(\mathbf{x}).$$

It turns out that the velocity is zero on  $\Gamma_{in}, \Gamma_w$  for the filtered snapshots  $\mathbf{u}(\mathbf{x}, t_i) - \bar{\mathbf{u}}(\mathbf{x}) - c(t_i)\mathbf{u}_c(\mathbf{x})$ , where for ease of notation we have renamed  $c(t)/c^*$  as  $c(t)$ . By substituting the

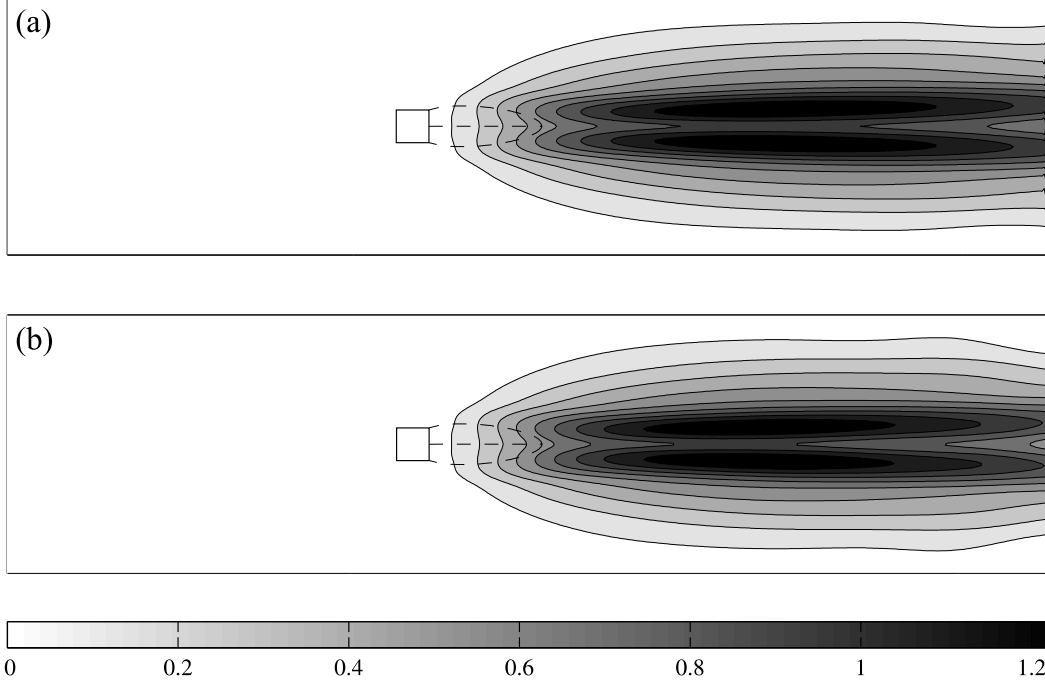


Figure 5: (a) Spatial distribution of the modulus of the unstable eigenvector (data courtesy of Flavio Giannetti). (b) Spatial distribution of the modulus of the reconstructed unstable eigenvector.

former expansion into the Navier-Stokes equations and projecting onto the POD modes one obtains:

$$\begin{aligned} \dot{a}_r(t) &= -(\nabla p, \phi_r) + A_r'' + C_{kr}'' a_k(t) - B_{ksr} a_k(t) a_s(t) - E_r'' \dot{c} - F_r'' c^2 + (G_r'' - H_{kr}'' a_k) c \\ a_r(0) &= (\mathbf{u}(\mathbf{x}, 0), \phi_r) \end{aligned}$$

where all the subscripts run from 1 to  $N_r$  and

$$\begin{aligned} E_r'' &= (\mathbf{u}_c, \phi_r) \\ F_r'' &= (\mathbf{u}_c \cdot \nabla \mathbf{u}_c, \phi_r) \\ G_r'' &= (\Delta \mathbf{u}_c, \phi_r) / Re - (\overline{\mathbf{u}} \cdot \nabla \mathbf{u}_c, \phi_r) - (\mathbf{u}_c \cdot \nabla \overline{\mathbf{u}}, \phi_r) \\ H_{kr}'' &= (\mathbf{u}_c \cdot \nabla \phi_k, \phi_r) + (\phi_k \cdot \nabla \mathbf{u}_c, \phi_r) \end{aligned}$$



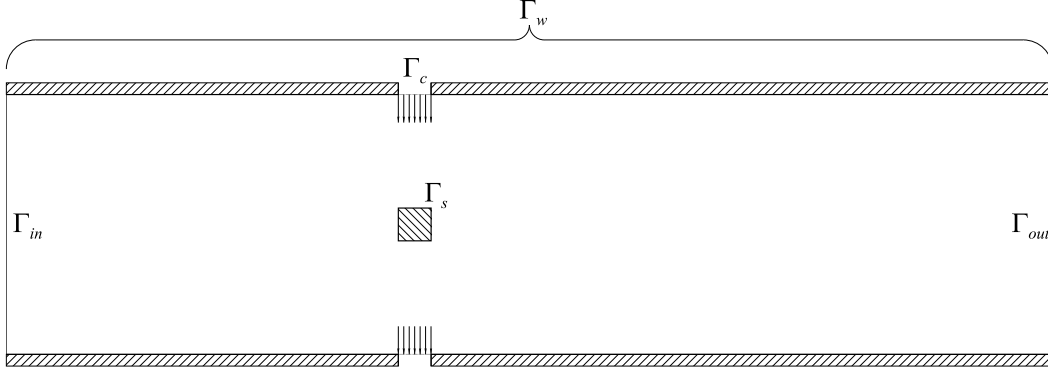


Figure 6: Actuation scheme

We choose to model the projection term relevant to the pressure and the unresolved scales by assuming that

$$-(\nabla p, \phi_r) = A'_r + C'_{kr} a_k(t) - E'_r \dot{c} - F'_r c^2 + (G'_r - H'_{kr} a_k) c$$

where the primed quantities are unknown. By setting  $A'_r = A_r - A''_r$ ,  $C'_{kr} = C_{kr} - C''_{kr}$ ,  $E'_r = E_r - E''_r$ ,  $F'_r = F_r - F''_r$ ,  $G'_r = G_r - G''_r$  and  $H'_{kr} = H_{kr} - H''_{kr}$ , the former system can be rewritten

$$\begin{aligned} \dot{a}_r(t) &= A_r + C_{kr} a_k(t) - B_{ksr} a_k(t) a_s(t) - E_r \dot{c} - F_r c^2 + (G_r - H_{kr} a_k) c \\ a_r(0) &= (\mathbf{u}(\mathbf{x}, 0), \phi_r) \end{aligned}$$

In other words the calibration procedure is performed for every projection term except for  $B_{ksr}$ .

We considered a numerical simulation at a Reynolds number of  $Re = 60$ , which is slightly greater than the critical value of 57. In this case the lift oscillates between -0.02 and 0.02 for the fully developed flow. Once the limit cycle has been reached, we set  $t = 0$  for the instant corresponding to zero lift and apply the following forcing law  $c(t) = -2/\pi \sin(2\pi t T_{ref}/T_S) \arctan(t T_{ref})$ , where  $T_S$  denotes the dimensional period of the limit cycle oscillations. In Fig. 7(a) both the lift and the forcing are shown as a function of the dimensional time.

A numerical database has been built by sampling the time span between 0 and 19.45 with 222 snapshots (see 'plus' markers in Fig. 7(a)) and a POD base of  $N_r = 5$  modes has been extracted from it with a reconstruction error of about 1.3%. The unknown  $A_r, C_{kr}, E_r, F_r, G_r$  and  $H_{kr}$  are determined according to the same procedure followed above for the modelling of the transient. The resulting direct-adjoint problem is then

$$\begin{cases} \dot{a}_r(t) = A_r + C_{kr} a_k(t) - B_{ksr} a_k(t) a_s(t) - E_r \dot{c} - F_r c^2 + (G_r - H_{kr} a_k) c \\ a_r(0) = (\mathbf{u}(\mathbf{x}, 0), \phi_r) \end{cases} \quad \text{direct problem}$$

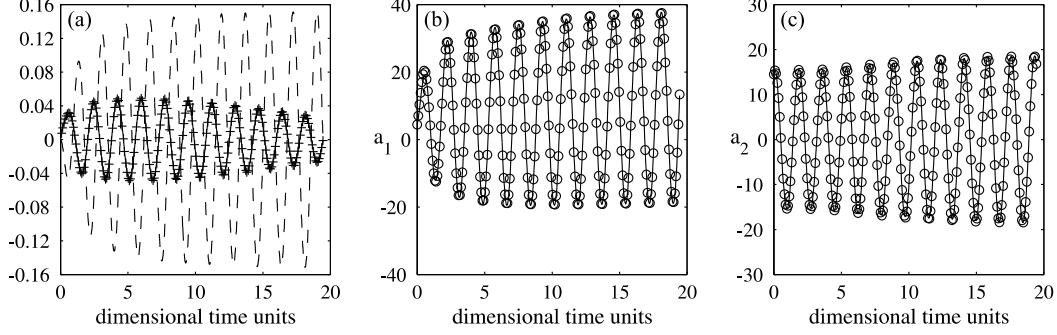


Figure 7: a) Lift versus time (“+”) and forcing law (dashed line); b) coefficient  $a_1$  and c) coefficient  $a_2$ : model integration (solid lines) and projection of the full numerical simulation (circles) versus time.

$$\begin{cases} -\dot{b}_r(t) = [C_{rk} - H_{rk}c(t) - (B_{lrk} + B_{rlk})a_l(t)] b_k(t) - 2[a_r(t) - \hat{a}_r(t)] \\ b_r(T) = 0 \end{cases} \quad \text{adjoint problem}$$

$$\begin{cases} \int_0^T b_r(t)dt = 0 \\ \int_0^T a_k(t)b_r(t)dt = 0 \\ \int_0^T b_k(t)\dot{c}(t)dt = 0 \\ \int_0^T b_k(t)c^2(t)dt = 0 \\ \int_0^T b_k(t)c(t)dt = 0 \\ \int_0^T a_k(t)b_r(t)c(t)dt = 0 \end{cases} \quad \text{optimality conditions}$$

that can be solved by means of the pseudo-spectral techniques employed previously. Typical results are depicted in Fig. 7(b) and (c), where the first two computed coefficient are compared successfully to the corresponding projections.

## 5 Conclusions

In this paper a pseudo-spectral method to obtain accurate low order models of transient phenomena has been described. The idea is to augment the POD-Galerkin model by a linear term whose coefficients are computed in order to fit a reference solution. The accuracy of the fitting is attained by a spectral representation of the low order model solution. This approach guarantees a virtually exact dynamical representation of the large scale structures.

It has been shown how the method can be employed to obtain a cheap and reasonably reliable surrogate to a full eigenmode analysis of the Navier-Stokes equations, when looking for the most unstable mode of a developing instability. An extension of this approach has been devised so as to encompass the modeling of flows under external actuation, providing a cheap and reliable plant model for control purposes. One of the main issues left open for investigation is how to take advantage of the perturbation analysis to efficiently modify the POD modes for flow regimes that are only slightly different from those used to generate the POD modes themselves. By doing so one would obtain a dramatic speed up in convergence to the optimal control when using for example the adaptive iterative procedure proposed in [18].

### Acknowledgements

We are grateful to Flavio Giannetti for providing the data reported in Fig. 5(a).

## References

- [1] N. Aubry, P. Holmes, J.L. Lumley, and E. Stone. The dynamics of coherent structures in the wall region of a turbulent boundary layer. *J. Fluid Mech.*, 192:115–173, 1988.
- [2] M. Bergmann, L. Cordier, and J.-P. Brancher. Optimal rotary control of the cylinder wake using POD reduced order model. *Phys. Fluids*, to appear, 2005.
- [3] M. Breuer, J. Bernsdorf, T. Zeiser, and F. Durst. Accurate computations of the laminar flow past a square cylinder based on two different methods: lattice-Boltzmann and finite-volume. *Int. J. of Heat and Fluid Flow*, 21:186–196, 2000.
- [4] C. Canuto, Y. Hussaini, A. Quarteroni, and T. Zang. *Spectral methods in fluid dynamics*. Springer, 1988.
- [5] W. Cazemier, R.W.C.P. Verstappen, and A.E.P. Veldman. Proper orthogonal decomposition and low-dimensional models for driven cavity flows. *Phys. Fluids*, 10:1685–1699, 1988.
- [6] M. Couplet, C. Basdevant, and P. Sagaut. Calibrated reduced-order POD-Galerkin system for fluid flow modelling. *J. Comp. Phys.*, 207:192–220, 2005.
- [7] R. W. Davis, E. F. Moore, and L. P. Purtell. Numerical-experimental study of confined flow around rectangular cylinders. *Phys. Fluids*, 27:46–59, 1984.
- [8] A. E. Deane, I. G. Kevrekidis, G. E. Karniadakis, and S. A. Orszag. Low-dimensional models for complex geometry flows: Application to grooved channels and circular cylinders. *Phys. Fluids A*, 3:2337–2354, 1991.
- [9] B. Galletti, C.H. Bruneau, L. Zannetti, and A. Iollo. Low-order modelling of laminar flow regimes past a confined square cylinder. *J. Fluid Mech.*, 503:161–170, 2004.

- [10] F. Giannetti and P. Luchini. Leading edge receptivity by adjoint methods. *J. Fluid Mech.*, to appear, 2005.
- [11] A. Iollo, A. Dervieux, J.A. Désidéri, and S. Lanteri. Two stable POD-based approximations to the Navier-Stokes equations. *Comput. Vis. Sci.*, 3(1-2):61–66, 2000.
- [12] A. Iollo, S. Lanteri, and J.A. Désidéri. Stability properties of POD-Galerkin approximations for the compressible Navier-Stokes equations. *Theor. Comp. Fluid Dyn.*, 13(6):377–396, 2000.
- [13] J. L. Lumley. The structure of inhomogeneous turbulent flows. In *Atmospheric Turbulence and Radio Wave Propagation*, edited by A. M. Yaglom and V. L. Tatarski, Moscow, pages 166–178, 1967.
- [14] X. Ma and G. E. Karniadakis. A low-dimensional model for simulating three-dimensional cylinder flow. *J. Fluid Mech.*, 458:181–190, 2002.
- [15] B. R. Noack, K. Afanasiev, M. Morzyński, G. Tadmor, and F. Thiele. A hierarchy of low-dimensional models for the transient and post-transient cylinder wake. *J. Fluid Mech.*, 497:335–363, 2003.
- [16] B.R. Noack, P. Papas, and P.A. Monkewitz. The need for a pressure-term representation in empirical Galerkin models of incompressible shear flows. *J. Fluid Mech.*, 523:339–365, 2005.
- [17] A. Okajima. Strouhal numbers of rectangular cylinders. *J. Fluid Mech.*, 123:379–398, 1982.
- [18] S. S. Ravindran. Control of flow separation over a forward-facing step by model reduction. *Comp. Meth. Appl. Mech. Eng.*, 191:4599–4617, 2002.
- [19] C. W. Rowley, T. Colonius, and R. M. Murray. Model reduction for compressible flows using pod and galerkin projection. *Physica D*, 189:115–129, 2004.
- [20] S. Sirisup and G.E. Karniadakis. A spectral viscosity method for correcting the long-term behavior of POD models. *J. Comp. Phys.*, 194:92–116, 2004.
- [21] L. Sirovich. Turbulence and the dynamics of coherent structures. Parts I,II and III. *Quart. Appl. Math.*, XLV:561–590, 1987.
- [22] H. Suzuki and Y. Inoue. Unsteady flow in a channel obstructed by a square rod (criss-cross motion of vortex). *Int. J. of Heat and Fluid Flow*, 14:2–9, 1993.
- [23] H. Telib, M. Manhart, and A. Iollo. Analysis and low-order modeling of the inhomogeneous transitional flow inside a T-mixer. *Phys. Fluids*, 8:2717–2731, 2004.



---

Unité de recherche INRIA Futurs  
Parc Club Orsay Université - ZAC des Vignes  
4, rue Jacques Monod - 91893 ORSAY Cedex (France)

Unité de recherche INRIA Lorraine : LORIA, Technopôle de Nancy-Brabois - Campus scientifique  
615, rue du Jardin Botanique - BP 101 - 54602 Villers-lès-Nancy Cedex (France)

Unité de recherche INRIA Rennes : IRISA, Campus universitaire de Beaulieu - 35042 Rennes Cedex (France)

Unité de recherche INRIA Rhône-Alpes : 655, avenue de l'Europe - 38334 Montbonnot Saint-Ismier (France)

Unité de recherche INRIA Rocquencourt : Domaine de Voluceau - Rocquencourt - BP 105 - 78153 Le Chesnay Cedex (France)

Unité de recherche INRIA Sophia Antipolis : 2004, route des Lucioles - BP 93 - 06902 Sophia Antipolis Cedex (France)

---

Éditeur  
INRIA - Domaine de Voluceau - Rocquencourt, BP 105 - 78153 Le Chesnay Cedex (France)  
<http://www.inria.fr>  
ISSN 0249-6399